A three-dimensional model of the human pulmonary acinus

Hiroko Kitaoka, Shinichi Tamura and Ryuji Takaki

J Appl Physiol 88:2260-2268, 2000.

J Appl Physiol
88: 2260–2268, 2000.

A three-dimensional model of the human pulmonary acinus

HIROKO KITAOKA,[1] SHINICHI TAMURA,[1], AND RYUJI TAKAKI[2]
[1]*Division of Functional Diagnostic Imaging, Osaka University Medical School, Suita City, Osaka 565-0871; and* [2]*Department of Engineering, Tokyo University of Agriculture and Technology, Tokyo 184-8588, Japan*

Kitaoka, Hiroko, Shinichi Tamura, and Ryuji Takaki. A three-dimensional model of the human pulmonary acinus. *J Appl Physiol* 88: 2260–2268, 2000.—A three-dimensional (3-D) model of the human pulmonary acinus, a gas exchange unit, is constructed with a labyrinthine algorithm generating branching ducts that fill a given space completely. Branching down to the third respiratory bronchioles is generated with the proposed algorithm. A subacinus, a region supplied by the last respiratory bronchiole, is approximated to be a set of cubic cells with a side dimension of 0.5 mm. The labyrinthine algorithm is used to determine a pathway through all cells only once, except at branching points with the smallest path lengths. In choosing each step of a pathway, random variables are used. Resulting labyrinths have equal mean path lengths and equal surface areas of inner walls. An alveolus can be generated by attaching alveolar septa, 0.25 mm long and 0.1 mm wide, to the inner walls. Total alveolar surface area and numbers of alveolar ducts, alveolar sacs, and alveoli in our 3-D acinar model are in good accordance with those reported in the literature.

pulmonary gas exchange; lung model; three-dimensional computer modeling; pulmonary labyrinth

THE STRUCTURE OF THE PULMONARY acinus, defined by Fletcher et al. (3) as a region of the lung distal to the terminal bronchiole (TB), is one of the most complicated in the human body. The TB branches into several respiratory bronchioles (RBs) in the acinus. The RB then branches into several alveolar ducts (ADs), which branch into several alveolar sacs (ASs, blind ends of the air pathway). The acinar structure is regarded as a branching ductal system filling the three-dimensional (3-D) space completely. The alveoli are open surfaces attached to the inner walls of RBs, ADs, or ASs. Therefore, the intra-acinar surface is topologically homeomorphic to one sheet, despite its complicated 3-D architecture.

Several morphometric studies of the pulmonary acinar structures have been carried out by making serial histological sections (6, 9, 11–13, 15) and by observing the casts (2, 4, 14). However, 3-D models of acinar structure have not been proposed. We propose a method to simulate the acinar structure by use of an algorithm generating an intra-acinar pathway. The basic idea of the algorithm is to construct a 3-D labyrinth, which starts from an entrance, passes every point only once, and includes branching. After construction of the labyrinth, alveoli are attached on its inner walls. From a requirement that the air transport should be effective, the algorithm should be designed so that the path lengths to each alveolus are the smallest. We call this algorithm a labyrinthine algorithm.

We previously proposed an algorithm to generate the airway tree down to TBs (10). The airway tree algorithm, i.e., the tree algorithm, divides the lung into numerous acini. According to Weibel (16), the TBs branch three times dichotomously within the acinus; hence, the acinus is divided into several subacini supplied by the last RBs. The intra-acinar pathway down to the last RBs can be given by the tree algorithm. ADs and ASs, which fill the subacinus, are given by the labyrinthine algorithm.

ALGORITHM GENERATING A 3-D LABYRINTH

We start with an assumption that the whole acinus can be approximated by a set of numerous cubic cells and that the intra-acinar pathway can be regarded as a sequence of cubic cells (Fig. 1). Therefore, construction of the pathway is locally limited only to extend straight or to turn at a right angle. An oblique pathway is approximated by a sequence of zigzag paths. We fix the cell size and the width of alveolar septa to 0.5 and 0.1 mm, respectively, and assign alveolar septa to be attached to the inner walls at 0.25-mm intervals (Fig. 1). These values are reasonable, since the outer and inner diameters of ADs and ASs are then 0.5 and 0.3 mm, respectively, which are consistent with the data previously reported (4, 17).

The labyrinthine algorithm is applied to the subacinus, the shape of which can be assumed to be a rectangle or more realistic forms given by the tree algorithm (10). The starting point of the labyrinth is chosen at a cell including the end point of the last RB. The basic idea of the algorithm is to determine a branching pathway that passes all cells only once, except at branching cells, without loop formation. The

The costs of publication of this article were defrayed in part by the payment of page charges. The article must therefore be hereby marked "*advertisement*" in accordance with 18 U.S.C. Section 1734 solely to indicate this fact.

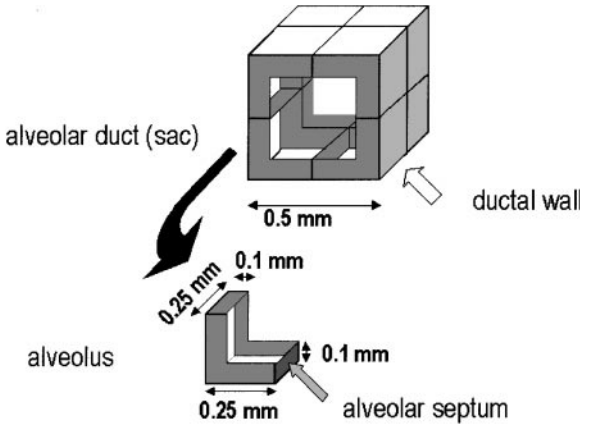

Fig. 1. Three-dimensional (3-D) alveolar model. There are 8 alveoli in a cubic cell with a side dimension of 0.5 mm. A 0.1-mm-wide alveolar septum is attached with inner walls at 0.25-mm intervals.

mean path length (MPL) from the starting point to all cells is required to be as small as possible.

First, we consider a rectangular subacinus consisting of $L \times M \times N$ cells. Figure 2 shows an example of a cubic subacinus made of $6 \times 6 \times 6$ cells. The starting point is assigned at a corner of the subacinus. Figure 3 shows some simple examples of labyrinthine walls and pathways at the lowest cross section (Fig. 2). The MPL becomes the largest when there is no branching (Fig. 3*A*). In this case, the pathway goes up to the second level at the *top left* cell. The MPL is calculated as $(LMN - 1)/2$. This is the least effective pathway. For derivation of MPL see APPENDIX A.

On the other hand, a simple example with the smallest MPL is shown in Fig. 3*B*, where branchings occur horizontally and vertically at every cell located on the left side and every branch ends at the right side. In this case, MPL is $(L + M + N - 3)/2$ (see below) and the number of ends is $L \times N$.

When the wall configuration is given as shown in Fig. 3*C*, the MPL remains unchanged, although the numbers of ends and branchings increase by 1.

It is obvious that the path length to each cell becomes larger when it includes detours, as shown in Fig. 3*D*. Here we define a detour as a route containing reverse directions. The MPL and the standard deviation (SD) are theoretically given by the following equations as long as there are no detours

$$\mathrm{MPL} = \left[\sum_{i=0}^{L-1} \sum_{j=0}^{M-1} \sum_{k=0}^{N-1} (i + j + k) \right] \Big/ LMN$$

$$= (L + M + N - 3)/2$$

$$\mathrm{SD} = \left\{ \left[\sum_{i=0}^{L-1} \sum_{j=0}^{M-1} \sum_{k=0}^{N-1} (i + j + k - \mathrm{MPL})^2 \right] \Big/ LMN \right\}^{1/2}$$

$$= [(L^2 + M^2 + N^2)/3]^{1/2}/2$$

In these formulas, the summations are taken for all paths. When $L = M = N$, $\mathrm{MPL} = 1.5(L - 1)$, and $\mathrm{SD} = 0.5L$.

Hence, we have constructed a labyrinthine algorithm generating a branching pathway without detours. When a cell has multiple directions, the direction generating a path is selected by a random process. Hence, this algorithm generates many kinds of labyrinths with the same MPL. The detail of the algorithm is explained in APPENDIX B.

There are no detours in any labyrinth generated with the above algorithm as long as the starting point is located at the corner. On the other hand, if the starting point is located inside the subacini, which is usual in an actual lung, we must modify the algorithm to avoid detours. Thus we have introduced a concept of priority direction for all *i*, *j*, and *k* axes according to the spatial relationship between the starting point and the center of the subacinus. Priorities are given to directions from the starting point to the center. Figure 4 shows priority directions for three different starting points. When several priority directions are possible, a direction is chosen randomly from them. If there is no priority direction, a direction is chosen randomly from possible nonpriority directions. This rule prevents activated cells from selecting directions that are the reverse of those from the starting point to themselves (see APPENDIX B).

Figure 5, *A* and *B*, shows examples of directions with and without priority. The starting points move from the corner toward the center of the subacinus by 1 for every direction. There are no detours in Fig. 5*A;* however,

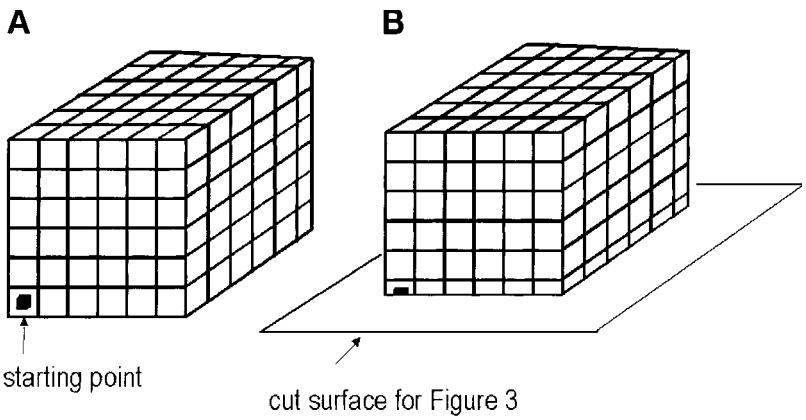

Fig. 2. Cubic subacinus with $6 \times 6 \times 6$ cells. *A*: outer appearance. *B*: cross section at lowest level shown in Fig. 3.

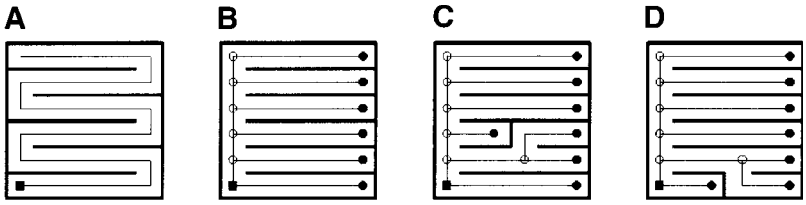

Fig. 3. Cross sections of cubic labyrinth starting at *bottom left*. ■, Starting points; ○, branching points; ●, end points. Paths are indicated by thin lines. *A*: case without branching, where mean path length to each cell (MPL) is largest. *B*: a simple example giving smallest MPL. Branchings occur at *left*, and end points are located at *right*. *C*: 1 more branching is added without changing MPL. *D*: branching with a detour, which has a larger MPL.

there are three detours in Fig. 5*B*, as shown in Fig. 5*C*, resulting in a longer MPL than in Fig. 5*A*. When a starting point is located at a corner, there is no cell in nonpriority direction from the starting point. Therefore, the algorithms with and without priority are the same in that case.

When the location of the starting point is shifted from the corner to the center by l, m, and n in the three directions, respectively, the MPL is calculated theoretically as follows

$$\mathrm{MPL} = [(L - l)^2 + l^2 - L + 2l]/2L + [(M - m)^2 + m^2 - M + 2m]/2M + [(N - n)^2 + n^2 - N + 2n]/2N$$

There is a very simple but important relationship between the number of inner walls and the number of cells. A cell along the pathway without branching has four walls. On the other hand, an end cell has five walls, and branching decreases the number of walls. For example, dichotomous and trichotomous cells have three and two walls, respectively. Because an increase in branching is associated with an increase in end cells, the total number of walls does not change by generating branching. Hence, for a sufficient number of the cells (N_c), we have the following relation with the number of inner walls (N_w) independent of the structure of the labyrinth

$$N_w = 4N_c$$

This means that the surface area of inner walls per unit volume is constant for any labyrinth structure. Because alveoli are attached along inner walls of the pathway, the number of alveoli and the total surface area of alveoli per unit volume should be constant.

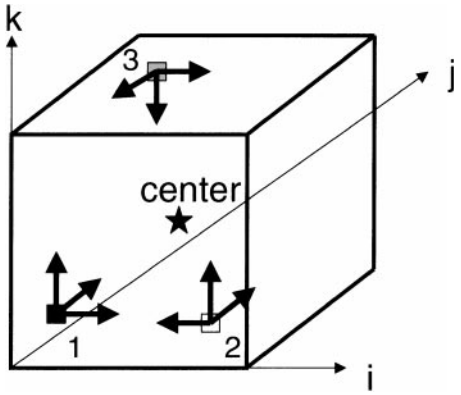

Fig. 4. Priority directions for 3 starting points.

There is another simple relationship between the total number of branches (B), the number of branching nodes (T), and the number of end points (E) in a branching tree structure as follows (8)

$$B = T + E$$

where the starting point is not regarded as an end point. This relationship is independent of whether branching is dichotomous, trichotomous, or quadrichotomous. In the human pulmonary subacinus, the trunk is the last RB, and the number of ASs is equal to E. On the other hand, the sum of the numbers of ADs and ASs is equal to B − 1. Therefore, the number of ADs is calculated as B − E − 1, which is equal to T − 1.

CHARACTERIZATION OF 3-D LABYRINTHS

We examined the characteristics of the 3-D labyrinth generated by our algorithm, first for a cubic subacinus and then for more realistic acinar contours generated by our airway tree algorithm (10).

Here, the acinar size is discussed. Acinar volumes have been investigated by several researchers. Hansen and Ampaya (5) and Kitaoka and Itoh (9) reported the average acinar volume at three-fourths total lung volume (TLV) as 183 and 173 mm^3, respectively. This means that the acinar volume is ~230 mm^3 at maximum inspiration. On the other hand, the airway tree generated by our algorithm contains 27,000 TBs within the TLV of 6.37 liters (10). According to Weibel (16), the lung parenchyma is 90% of TLV. Hence, the average acinar volume at the maximum inspiration in our airway tree model is calculated as 212 mm^3 (= 6.37 × 10^6 × 0.9/27,000). This value is close to those obtained with the fixed lungs mentioned above. Finally, we assigned the average acinar volume as 216 mm^3, which corresponds to a cube with a side dimension of 6 mm.

When a 0.1-mm-wide alveolar septum is attached to the inner walls at 0.25-mm intervals, as mentioned

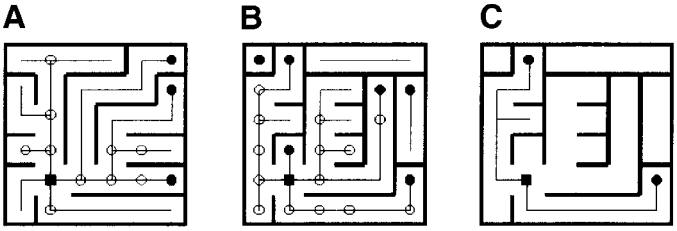

Fig. 5. Paths of cubic labyrinth, where starting cell is shifted from corner toward center of labyrinth by 1 unit in all directions. Cross section is at 2nd level. *A*: case with priority direction, where no detours are recognized. *B*: case without priority direction allowing 3 detours. *C*: pickup of 3 detours in *B*.

above, one cell contains eight alveoli on average. The surface area of one alveolus is calculated as 0.255 mm^2 (= 0.25 × 0.25 × 2 + 0.25 × 0.1 × 4 +0.15 × 0.1 × 2), and the alveolar surface area per cell is calculated as 2.04 mm^2 (= 0.255 × 8). Because the volume of one cell is 0.125 mm^3, the number and the total surface area of alveoli per unit volume of lung parenchyma are calculated as 64/mm^3 (= 8/0.125) and 16.3 mm^2/mm^3 (= 2.04/0.125), respectively. The total number of alveoli and the total surface area with TLV of 6.37 liters are then estimated as 370 × 10^6 (= 6.37 × 10^6 × 0.9 × 64) and 93.4 m^2 (= 6.37 × 0.9 × 16.3), respectively, which are in good accordance with the data previously reported (1, 5, 7, 13, 17).

Cubic subacinar model. As a model of subacinus, we assumed a cube with a side dimension of 3.0 mm, which contains 6^3 = 216 cells. First, we assigned the starting cell at a vertex. The MPL is always 3.75 ± 1.5 (SD) mm, equal to the theoretical values as mentioned above. Under the assumption that lengths of all RBs in the acinus are 1.5 mm, the MPL from the first RB is calculated to be 8.25 ± 1.5 mm. These values are in good accordance with the morphometric data of Haefeli-Bleuer and Weibel (4), who reported 8.8 ± 1.4 mm.

Next, we assigned the starting point inside the subacinus (Fig. 4). We performed 200 trials with and without priorities. When priorities were given, MPL was always equal to the theoretical value, 2.75 mm. On the other hand, MPL without priorities became >2.75 mm and ranged from 2.79 to 3.14 mm.

The numbers of ADs and ASs are equal to E and T − 1, respectively, as mentioned above. These numbers are different at every trial because of random processes. We performed 200 trials and examined distributions of these numbers. The number (mean ± SD) of ADs was 37.2 ± 2.3 (range 33–41), whereas the number of ASs was 49.4 ± 1.3 (range 46–51). These values are also consistent with those reported previously (4, 12).

Figure 6 shows the 3-D structure of the pathway and alveolar walls within the subacinus for the case shown in Fig. 5*A*. Figure 6*A* is the whole pathway, and Fig. 6*B* is a sketch indicating connectivity of the branching

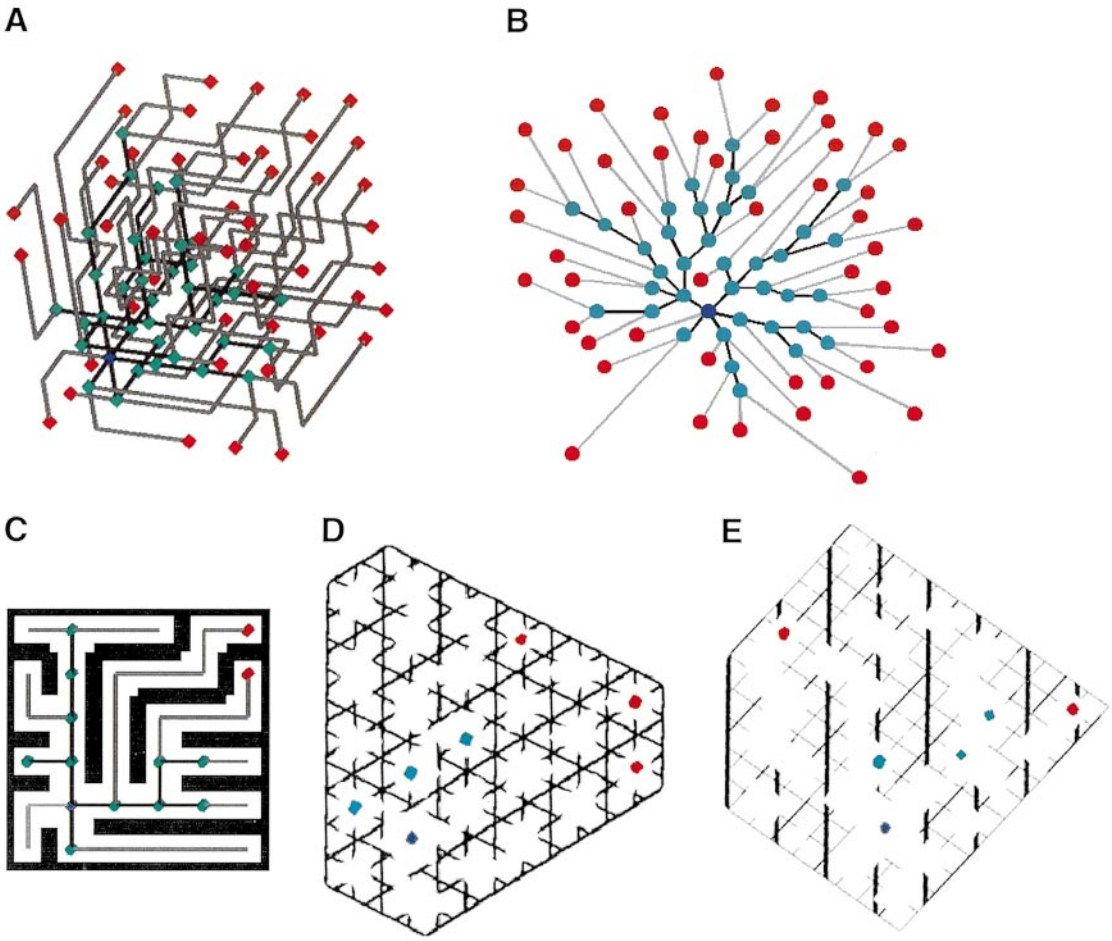

Fig. 6. 3-D presentations of pathway and alveolar walls of cubic subacinus in Fig. 5*A*. *A*: 3-D structure of whole pathway. Alveolar ducts (ADs) and alveolar sacs (ASs) are drawn with black and gray lines, respectively. Starting point, branching points, and end points are blue, green, and red, respectively. *B*: connectivity diagram of pathway. *C*–*E*: 3 cross sections of alveolar walls. Cross section in *C* is the same as Fig. 4*A*. All alveolar walls are parallel or perpendicular to cross section. *D*: cross section perpendicular to line connecting 2 opposite vertices of cube. ADs and ASs are presented as hexagons. *E*: cross section with direction between those in *D* and *C*. Alveolar walls are presented as parallelograms.

structure of the pathway, a connectivity diagram. The resulting lengths of ADs and ASs are, respectively, shorter and longer than morphometric data of actual pulmonary acini (4, 12) because of frequent branchings at the proximal parts. However, the branching pattern and the total path length are consistent with the values previously reported (4, 12). Figure 6, *C–E*, shows alveolar walls on three different cross sections passing the starting point. In Fig. 6*C*, the cross section is parallel to the alveolar walls, as in Fig. 5*A*. When the cross sections are oblique, as in Fig. 6, *C* and D, the alveolar shapes give, for example, a hexagon (Fig. 6*D*) and tetragon (Fig. 6*E*). Hexagonal ductal walls with alveolar septa in Fig. 6*D* are very similar to those in real histological sections of the lung.

From these results, we can conclude that our labyrinthine algorithm with priority of directions is suitable for modeling the effective air pathway.

Acinar models with realistic boundaries. We generated an airway tree model down to the last RBs supplying subacini with the tree algorithm. Each subacinus was approximated by a set of cubic cells with side dimension of 0.5 mm, and the labyrinthine algorithm with priorities was applied to it.

We show three acinar models in Figs. 7 and 8 and Table 1. Figure 7 shows *model A*, consisting of eight subacini. The total volume is 256 mm^3, which is somewhat larger than the average in actual cases. Figure 7, *A* and *B*, shows the outer appearance and the cross section, respectively. Figure 7, *C–E*, shows the intra-acinar pathways. The view in Fig. 7*C* is the same as in Fig. 7*A*; the view angle in Fig. 7*D* is slightly different. Figure 7*E* shows the pathway of the subacinus. The intra-acinar pathway is radially extended from the end of the RB. Although the shape of the subacinus is irregular, there is no detour or loop in the pathway. Its connectivity diagram is shown in Fig. 7*F*. The volume of the subacinus is 40 mm^3, and the MPL from the starting point is 2.7 mm. The numbers of ADs and ASs are 68 and 83, respectively.

Figure 8 shows a combination of *models B* and *C;* TBs arise from the same pre-TB. They consist of seven and five subacini, respectively. The morphometric data of *models A*, *B*, and *C* are summarized in Table 1. *Models B* and *C* have larger MPL than *model A*, because the acinar shapes of *models B* and *C* are more anisotropic.

DISCUSSION

Results of our model analysis have shown that our labyrinthine algorithm leads to reasonable predictions of some characteristic quantities in the human pulmonary acinus. Here we compare these predictions more precisely with past studies.

Detailed morphometric studies of intra-acinar structures were performed by Parker et al. (12), Hansen et al. (6), and Haefeli-Bleuer and Weibel (4). According to these studies, the TB branches three times with nearly symmetric dichotomy, and the last RB branches 2–12 times with asymmetric dichotomy. Parker, Hansen, and Haefeli-Bleuer and their co-workers reported an average of 6, 8, and 7 branchings of the TB from the last RB to ASs, respectively, and ~800, 4,900, and 2,000 ADs and ASs per acinus, respectively. The deviations in these values may be due to difficulties of shape definition for irregular branching structures. Number and size of segments in a branching system depend on the definition of branching. If one regards a slight protrusion of an AD as a branched AS, the branching times and the number of ASs would increase. In fact, the number of ASs reported by Hansen et al. is much larger than that reported by Parker et al. Hansen et al. estimated that the average number of alveoli per AS was 3.5, whereas Parker et al. estimated the number to be 13 (there was no statement about the alveolar number in the report of Haefeli-Bleuer and Weibel). The ratio 3.5/13 is approximately reciprocal to the ratio of their numbers of ASs (2,500/400). Our acinar *model A* has an average of 398 ADs and 468 ASs, and the average number of alveoli per AS is 18. These values are close to those reported by Parker et al. (12).

Haefeli-Bleuer and Weibel (4) estimated the path length through the intra-acinar airway and reported an MPL of 8.8 ± 1.4 mm from the first RB to ASs. The values in our *models A* and *B* are in good accordance with their values. *Model C* has a larger MPL because of its long shape. In all our models, numbers of ADs and ASs are almost proportional to the acinar volume. These values are within the range of values previously reported (4, 5, 12).

There are limitations of our 3-D acinar model. We have assumed that the intra-acinar pathway is a sequence of cubic cells and that construction of the pathway is limited only to extend straight or to turn at a right angle; hence, the geometry of the intra-acinar pathway is locally unrealistic. However, the whole pathway can simulate an oblique or a curved branching system well. This kind of discrete approximation is convenient for computer simulation. Another limitation in our model is that all alveoli are assumed to be congruent. However, it is possible to regard the alveolar size as one of the variables representing the state of the alveoli. Hence, we do not regard these limitations as serious. We have preliminarily succeeded in simulating remodelings of acinar structures in idiopathic interstitial pneumonia and pulmonary emphysema. The acinar model presented here will enable us to simulate respiratory diseases and give us a better understanding of the structural-functional correlation of the lung.

Conclusion. Our labyrinthine algorithm reproduces well the intra-acinar pathway, despite its simplicity. Moreover, it is expected that the 3-D acinar model generated by this algorithm might enable us to simulate respiratory diseases and to understand the structural-functional correlation of the lung.

APPENDIX A

MPL from the starting point to all cells in a rectangle space. The location of a cell is denoted C(i,j,k), as shown in Fig. 2, where $0 \leq i \leq L - 1$, $0 \leq j \leq K - 1$, and $0 \leq k \leq N - 1$. The

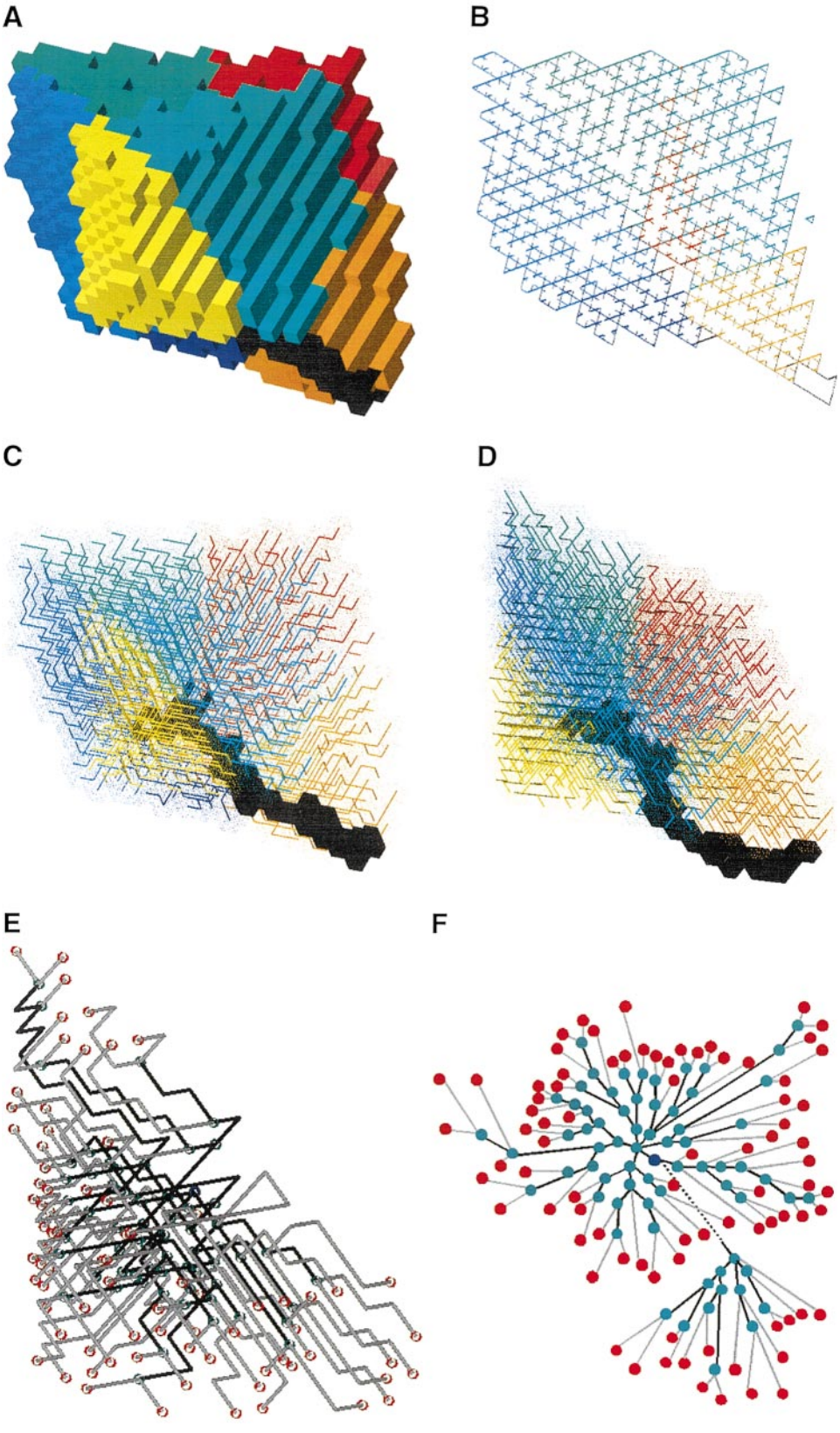

Fig. 7. Acinar *model A* consisting of 8 subacini. Bronchioles are black, and alveolar walls are different colors according to subacini. *A*: outer appearance of acinus approximated by a set of cubes with side dimension of 0.5 mm. *B*: a thin layer with thickness of 0.02 mm cut from acinus. *C* and *D*: all pathways within acinus. Alveolar walls are indicated with tiny dots. View angles of *C* and *A* are the same, but view angle of *D* is slightly different. *E*: pathway within 1 subacinus (yellow in *A*). *F*: connection diagram of pathway within yellow subacinus.

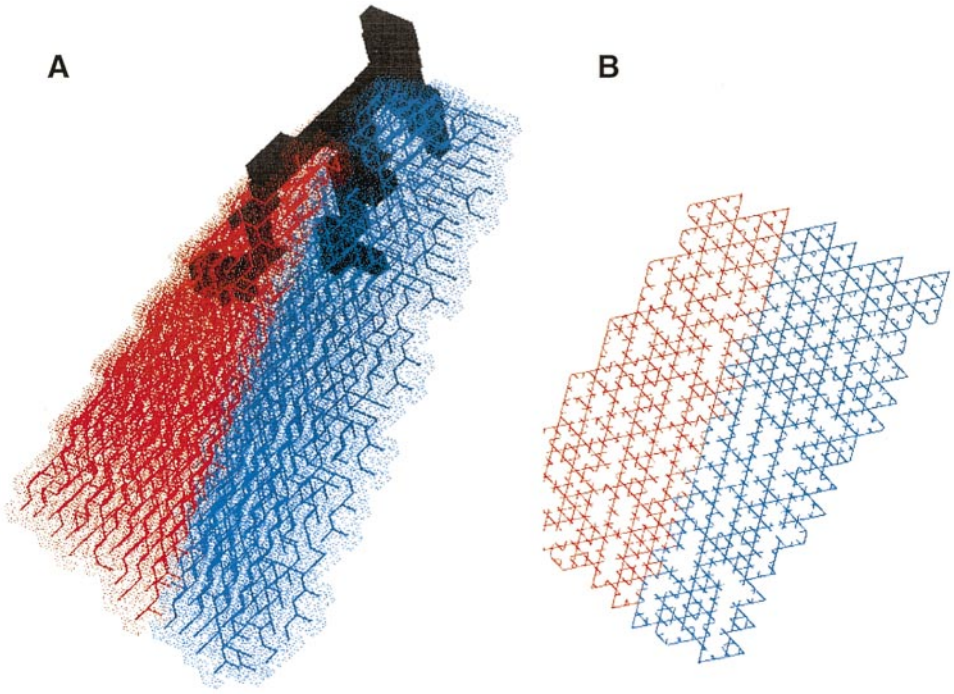

Fig. 8. Acinar *models B* (blue) and *C* (pink). Terminal bronchioles (TBs) of *models B* and *C* arise from the same pre-TB. *A*: outer appearance of *models B* and *C*. Shapes are more elongated than shape of *model A*. *B*: thin layer with thickness of 0.02 mm cut from acini.

path length from the starting point, $C_0(i_0,j_0,k_0)$, to the cell $C(i,j,k)$ is denoted $P(i,j,k)$

$$P(i_0,j_0,k_0) = 0,$$

$$MPL = \left[\sum_{i=0}^{L-1}\sum_{j=0}^{M-1}\sum_{k=0}^{N-1} P(i,j,k)\right] \Big/ LMN$$

In the case of Fig. 3*A*, path lengths increase one-by-one from 1 to the maximum value $LMN - 1$. Therefore, we have

$$MPL = \left(\sum_{p=0}^{LMN-1} p\right) \Big/ LMN = (LMN - 1)/2$$

In the case of Fig. 3*B*, path lengths in the first line on the first level are 0, 1, 2, 3, 4, and 5, respectively. Those in the second line on the first level are 1, 2, 3, 4, 5, and 6, respectively, and so on. On the second level, the path length of each cell increases by one from that on the first level, and so on. Therefore , $P(i,j,k) = (i + j + k)$, and we have

$$MPL = \left[\sum_{i=0}^{L-1}\sum_{j=0}^{M-1}\sum_{k=0}^{N-1} P(i,j,k)\right] \Big/ LMN$$

$$= \left[\sum_{i=0}^{L-1}\sum_{j=0}^{M-1}\sum_{k=0}^{N-1} (i + j + k)\right] \Big/ LMN = (L + M + N - 3)/2$$

In general, $P(i,j,k)$ is always equal to $(i + j + k)$ as long as the starting point is at the corner and there are no detours. In Fig. 3*C*, the pathway of the cell at the right side of the newly made wall is the same as in Fig. 2*B*.

Table 1. *Morphometry of 3-D acinar model*

Model	Volume, mm^3	Path Length, mm	Number of ADs	Number of ASs	Number of Alveoli	Surface Area of Alveolar Wall, mm^2
A	256	8.2 ± 2.3	398	463	17.4×10^3	4.53×10^3
B	176	8.6 ± 2.6	272	298	11.3×10^3	2.93×10^3
C	167	9.6 ± 2.2	253	290	10.7×10^3	2.77×10^3

Values for path length are means ± SD. 3-D, 3-dimensional; ADs, alveolar ducts; ASs, alveolar sacs.

APPENDIX B

Labyrinthine algorithm. The algorithm generating a branching pathway is constructed with a method of queue ordering cells. The queue is a linear array of cells that can generate paths. At every step, only a cell located at the front of the queue can generate one path by selecting one of the possible directions. We call this cell an "activated cell." When an adjacent cell is already passed, the direction toward that cell is forbidden to prevent loop formation. If the activated cell has no possible direction, it is deleted from the queue. If it has only one possible direction, it generates one step of path and is then deleted from the queue. If it has more than one possible direction, it generates one step and is then put at the rear of the queue. The cell connected with the activated cell via a newly produced path is put at the rear of the queue. Thus paths are generated sequentially until the queue becomes empty. The number of paths is always equal to the cell number minus 1, because there is no loop.

Figure 9 shows an example of paths in a space with $3 \times 3 \times 1$ cells. Because the activated cells continue to be shifted outward from the starting point, there is no chance for activated cells to select backward directions. Therefore, there are no detours in the constructed pathway.

Figure 10 shows cases without and with priority directions with $4 \times 4 \times 1$ cells. In Fig. 10*A*, the activated cell at the seventh step with number 6 has a possible upward direction, which leads to a detour. However, in Fig. 10*B*, cells located in the priority directions can select only the priority directions. Likewise, cells located opposite the priority directions can select only opposite directions. Therefore, in the case with priority directions, there is no chance for all activated cells to make detours.

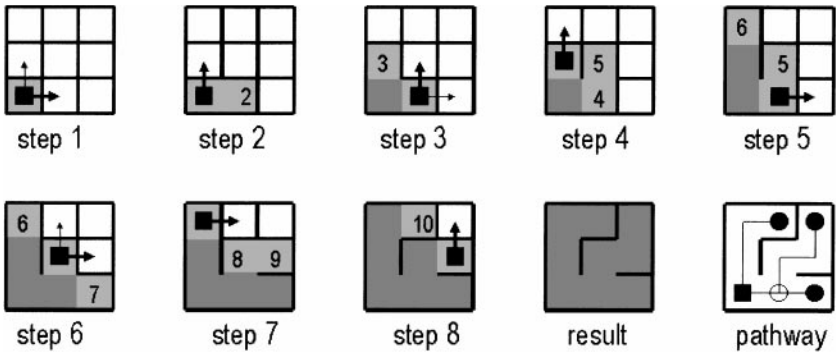

Fig. 9. Labyrinthine algorithm in $3 \times 3 \times 1$ rectangular subacinus. Starting point is at *bottom left*. Activated cells are indicated with squares at respective steps. Possible directions are indicated with arrows. For cells with >1 possible direction, selected direction is indicated by thicker arrow. Numbers within diagrams show orders within queue for activation; *step 1* is starting cell. Dark cells have no possible directions. After *step 8*, a branching labyrinth without loops or detours is constructed. Constructed pathway is indicated by thin lines. ○, Branching points; ●, end points.

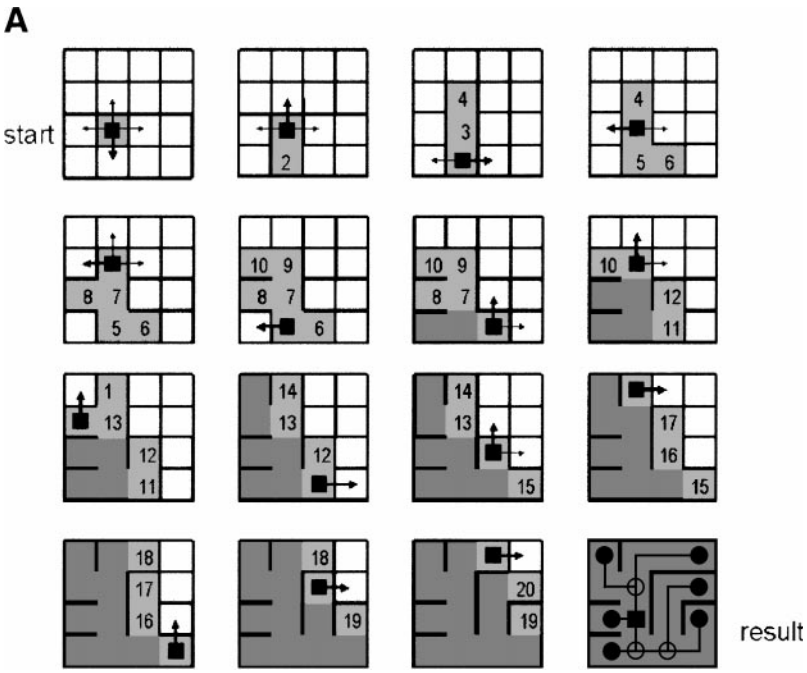

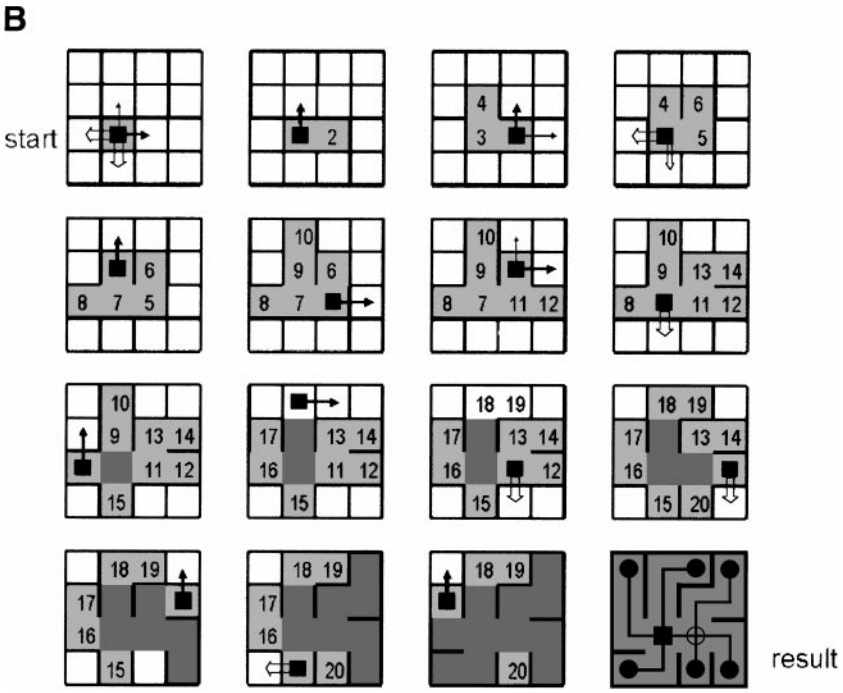

Fig. 10. Labyrinthine algorithm in $4 \times 4 \times 1$ rectangular subacinus, where starting point is inside space without (*A*) and with (*B*) priority directions. In *A*, 2 detours are generated; there are no detours in *B*. In this case, priority directions are in positive directions in *i* and *j* axes. Priority and nonpriority possible directions are indicated with solid and open arrows, respectively. Nonpriority possible directions are not indicated if there are prior possible directions, except at *start*. For cells with >1 possible direction, selected direction is indicated by thicker arrow.

This algorithm is applicable to an acinus with any shape as long as it is approximated by a set of cubic cells.

Address for reprint requests and other correspondence: H. Kitaoka, Div. of Functional Diagnostic Imaging, Osaka University Medical School, 2-2 Yamadaoka, Suita City, Osaka 565–0871, Japan (E-mail: kitaokah@image.med.osaka-u.ac.jp).

Received 29 July 1999; accepted in final form 25 January 2000.

REFERENCES

1. **Angus GE and Thurlbeck WM.** Number of alveoli in the human lung. *J Appl Physiol* 32: 483–485, 1972.
2. **Boyden EA.** The structure of the pulmonary acinus in a child of six years and eight months. *Am J Anat* 132: 275–300, 1971.
3. **Fletcher CM, Gilson JG, Hugh-Jones P, and Scadding JG.** Terminology, definitions, and classification of chronic pulmonary emphysema and related conditions: a report of the conclusions of a CIBA symposium. *Thorax* 14: 286–299, 1959.
4. **Haefeli-Bleuer B and Weibel ER.** Morphometry of the human pulmonary acinus. *Anat Rec* 220: 401–414, 1988.
5. **Hansen JE and Ampaya EP.** Human air space shape, sizes, areas, and volumes. *J Appl Physiol* 38: 990–995, 1975.
6. **Hansen JE, Ampaya EP, Gordon HB, and Navin JJ.** Branching pattern of airways and air spaces of a single human terminal bronchiole. *J Appl Physiol* 38: 983–989, 1975.
7. **Kitaoka H.** Numerical density of alveoli in the human lung—measurement using serial thin slices as three-dimensional probes. *Tohoku J Exp Med* 170: 45–52, 1993.
8. **Kitaoka H, Burri PH, and Weibel ER.** Development of the human fetal airway tree: analysis of the numerical density of airway endtips. *Anat Rec* 244: 207–213, 1996.
9. **Kitaoka H and Itoh H.** Computer-assisted three-dimensional volumetry of the human pulmonary acini. *Tohoku J Exp Med* 167: 1–12, 1992.
10. **Kitaoka H, Takaki R, and Suki B.** A three-dimensional model of the human airway tree. *J Appl Physiol* 87: 2207–2217, 1999.
11. **Mercer RR and Crapo JD.** Three-dimensional reconstruction of the rat acinus. *J Appl Physiol* 63: 785–794, 1987.
12. **Parker H, Horsfield K, and Cumming G.** Morphology of distal airways in the human lung. *J Appl Physiol* 31: 386–391, 1971.
13. **Pump KK.** Morphology of the acinus of the human lung. *Dis Chest* 56: 126–134, 1969.
14. **Schreider JP and Raabe OG.** Structure of the human respiratory acinus. *Am J Anat* 162: 221–232, 1981.
15. **Stelter GP, Hansen JE, and Fairchild DG.** A three-dimensional reconstruction of lung parenchyma. *Am Rev Respir Dis* 94: 79–85, 1966.
16. **Weibel ER.** *Morphometry of the Human Lung.* New York: Academic, 1963.
17. **Weibel ER.** Design of airways and blood vessels considered as branching trees. In: *The Lung: Scientific Foundations.* New York: Raven, 1991, p. 711–720.